Characterization of the Heme Environmental Structure of Cytoglobin, a Fourth Globin in Humans†

Hitomi Sawai,‡,§ Norifumi Kawada,|| Katsutoshi Yoshizato,⊥ Hiroshi Nakajima,@ Shigetoshi Aono,@ and Yoshitsugu Shiro*,§

Department of Life Science, Graduate School of Science, Himeji Institute of Technology, 3-2-1 Kouto, Kamigori-cho, Ako, Hyogo 678-1297, Japan, Department of Hepatology, Graduate School of Medicine, Osaka City University, 1-4-3 Asahi-machi, Abeno-ku, Osaka 545-8585, Japan, Developmental Biology Laboratory, Department of Biological Science, Graduate School of Science, Hiroshima University, 1-3-1 Kagamiyama, Higashihiroshima, Hiroshima 739-8526, Japan, Tissue Regeneration Project, Hiroshima Prefecture Collaboration of Regional Entities for the Advancement of Technological Excellence, Japan Science and Technology Corporation, 3-10-32, Kagamiyama, Higashihiroshima, Hiroshima 739-006, Japan, School of Materials Science, Japan Advanced Institute of Science and Technology, 1-1 Asahidai, Tatsunokuchi, Ishikawa 923-1292, Japan, and RIKEN Harima Institute/SPring-8, 1-1-1 Kouto, Mikazuki-cho, Sayo, Hyogo 679-5148, Japan

Received October 25, 2002; Revised Manuscript Received January 14, 2003

ABSTRACT: Cytoglobin (Cgb) represents a fourth member of the globin superfamily in mammals, but its function is unknown. Site-directed mutagenesis, in which six histidine residues were replaced with alanine, was carried out, and the results indicate that the imidazoles of His81 (E7) and His113 (F8) bind to the heme iron as axial ligands in the hexacoordinate and the low-spin state. The optical absorption, resonance Raman, and IR spectral results are consistent with this conclusion. The redox potential measurements revealed an E' of 20 mV (vs NHE) in the ferric/ferrous couple, indicating that the imidazole ligands of His81 and His113 are electronically neutral. On the basis of the ν_{Fe-CO} and ν_{C-O} values in the resonance Raman and infrared spectra of the ferrous−CO complexes of Cgb and its mutants, it was found that CO binds to the ferrous iron after the His81 imidazole is dissociated, and three conformers are present in the resultant CO coordination structure. Two are in closed conformations of the heme pocket, in which the bound CO ligand interacts with the dissociated His81 imidazole, while the third is in an open conformation. The ν_{Fe-O_2} in the resonance Raman spectra of oxy Cgb can be observed at 572 cm^{-1}, suggesting a polar heme environment. These structural properties of the heme pocket of Cgb are discussed with respect to its proposed *in vivo* oxygen storage function.

Stellate cell activation-associated protein (STAP)[1] is a hemoprotein that was recently discovered on the basis of a proteomics analysis of rat stellate cells, liver specific pericytes (*1*). The molecular mass of STAP is ∼21 kDa, and its amino acid sequence is ∼25∼40% identical to those of some globins, such as myoglobin, hemoglobin α- and β-chains, lamprey hemoglobin, etc. In addition, key amino acid residues that are conserved among a variety of globins are also present in its sequence (Figure 1A). Therefore, STAP has been identified as a fourth globin in mammals, after myogobin (Mb), hemoglobin (Hb), and neuroglobin (Ngb). Indeed, the recombinant protein of STAP expressed in *Escherichia coli* contains a heme (Fe-protoporphyrin) as a prosthetic group, and thus gives optical absorption spectra characteristic of hemoproteins.

Since STAP was initially identified in fibrotic liver tissues induced by the administration of thioacetamide (*2*), it was concluded that this hemoprotein might play a crucial role in the development of liver fibrosis. STAP is dramatically induced in *in vivo*-activated stellate cells isolated from fibrotic liver and in stellate cells undergoing *in vitro* activation during primary culture. This induction was observed along with that of other activation-associated molecules, such as smooth muscle α-actin, PDGF receptor-β, and the neural cell adhesion molecule. In our immunoelectron microscopy and proteome analysis, STAP could be detected in stellate cells but not in other hepatic constituent cells (*2*). However, recent reports indicate that the same type of globin is present in a variety of tissues of other mammalian organs, and this globin has been independently designated as histoglobin (*3*) or cytoglobin (*4*). Therefore, STAP is not globin specific to fibrotic liver tissue, but constitutively exists in other tissues of mammals in addition to liver. For this reason, we hereafter designate this specific globin as cytoglobin (Cgb).[2] An examination of the physiological functions of Cgb on the basis of its molecular structure would be highly desirable.

† This work was supported by in part by the Structural Biology and Molecular Ensemble Programs in RIKEN (to Y.S.) and by Grants-in-Aid for Scientific Research from the Ministry of Education, Science, Culture and Sports of Japan.

* To whom correspondence should be addressed. E-mail: yshiro@mailman.riken.go.jp.

‡ Himeji Institute of Technology.

§ RIKEN Harima Institute/SPring-8.

|| Osaka City University.

⊥ Hiroshima University.

@ Japan Science and Technology Corporation and Japan Advanced Institute of Science and Technology.

[1] Abbreviations: STAP, stellate cell activation-associated protein; Hb, hemoglobin; Mb, myoglobin; IR, infrared; Ngb, neuroglobin; Cgb, cytoglobin; cyt b_5, cytochrome b_5; CD, circular dichroism; HemAT-Bs, HemAT from *Bacillus subtilis*.

10.1021/bi027067e CCC: $25.00
Published on Web 04/11/2003

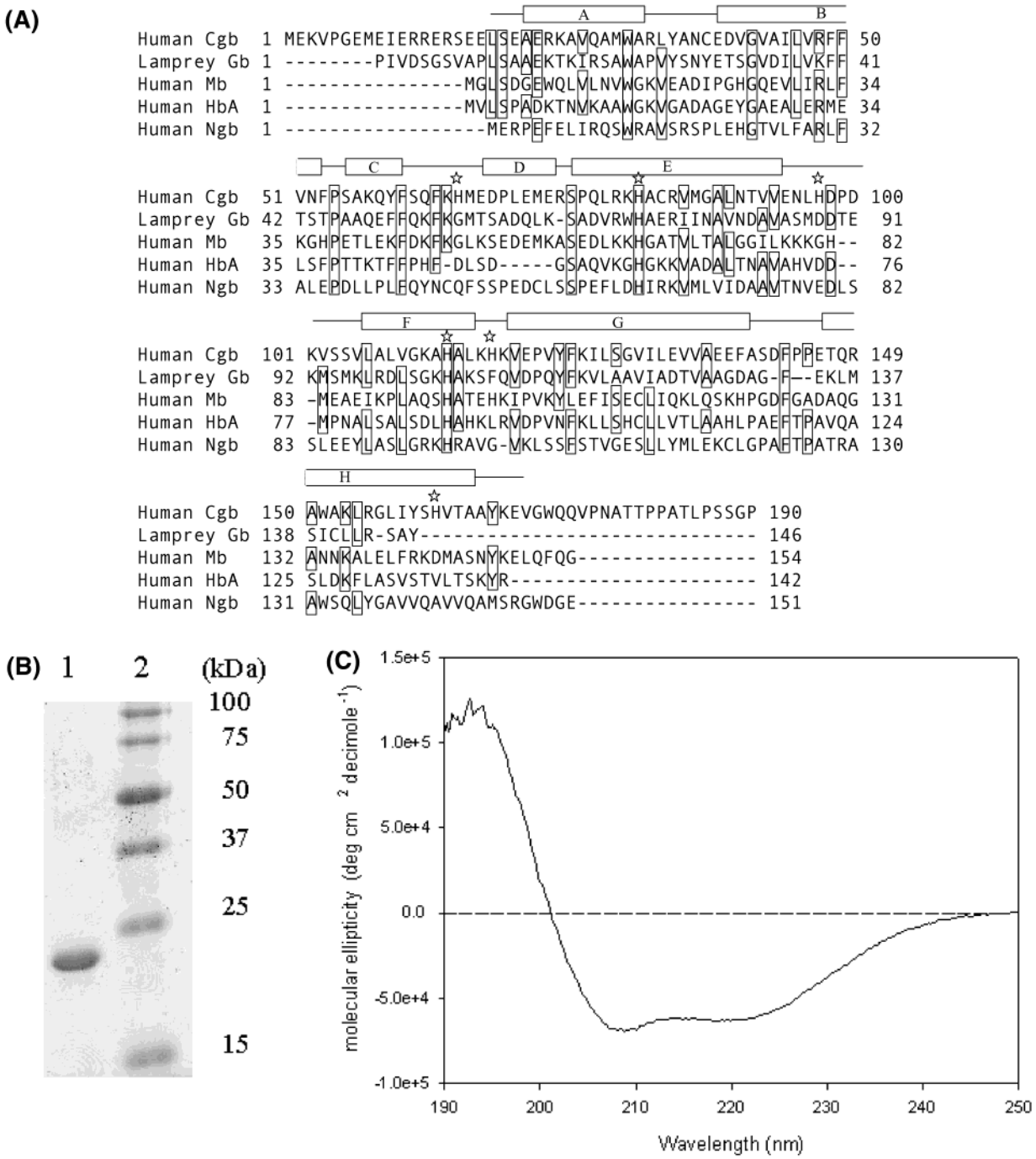

FIGURE 1: (A) Alignment of the amino acid sequence of human cytoglobin (Cgb) with those of lamprey globin (Gb), human myoglobin (Mb), the human hemoglobin α-chain (HbA), and human neuroglobin (Ngb). Highly conserved residues among the globins are bordered. Histidine residues changed by site-directed mutagenesis are denoted with asterisks. The secondary structure of Cgb was proposed, and α-helices are shown as boxes A−H by LIBRA-I. (B) Finally purified nontag Cgb run on lane 1 of SDS−PAGE. Lane 2 contained a molecular mass marker. (C) CD spectrum of Cgb in 50 mM Tris-HCl buffer at pH 8.0.

Cgb in the ferric and ferrous states exhibits optical absorption spectra characteristics that indicate heme coordinated to two histidyl imidazole groups as axial ligands (*3*). This structural feature is not identical to those of Hb and Mb, but the same as those of "hexacoordinate" Hbs recently found in animals, protists, cyanobacteria, and all plants (*5*−*12*). Hargrove and co-workers reported the crystal structure of one of the hexacoordinate Hbs, Hb found in nonsymbiotic plants (riceHb1), determined at 2.4 Å resolution (*13*), whose optical spectral properties strongly resemble those of Cgb. In riceHb1, the F8 histidine as well as the E7 histidine residues are directly coordinated to the heme iron as fifth and sixth ligands, respectively. A structural comparison between riceHb1 and sperm whale Mb suggested dramatic conformational changes of riceHb1 upon binding of the external ligand (CO, O_2, etc.). When the ligand binds at the iron coordination site, the imidazole side chain of His E7 dissociates and moves with concomitant upward and

[2] The name of this globin protein is still controversial. We will discuss the nomenclature in detail elsewhere on the basis of the localization of this protein in tissues of all organs (N. Kawada et al., manuscript in preparation).

outward movement of the E helix. The resultant position of His E7 imidazole would be similar to that seen for the distal His in sperm whale Mb. On the other hand, three hypotheses have been put forward so far, with respect to the function of the hexacoordinate Hbs (*5*−*17*). First, they might serve as O_2 transport proteins that sequester O_2 under hypoxic conditions and facilitate its diffusion to cells that require aerobic mitochondrial respiration. Second, they might serve as NADH oxidases that facilitate the glycolytic generation of ATP under microaerobic conditions. Third, they might act as O_2-sensing proteins that undergo a substantial conformational change in response to ligand binding or release, and this conformational change could activate other proteins or enzymes that have specific regulatory functions.

Cgb, and neuroglobin (Ngb), both of which are present in mammalian tissues, can be classified as members of the newly discovered class of hexacoordinate Hbs. Since their spectral features are similar, both vertebrate globins might be involved in physiological actions, as is the case for invertebrate and nonsymbiotic plant Hbs (*14*, *15*), but this has not yet been clearly established. On the other hand, the ligand binding equilibrium and kinetics reported recently are notably different between Cgb and Ngb (*16*, *17*), implying differences in their physiological functions. The environment experienced by heme-bound ligands is critical for the function of globins, since it controls the kinetics of ligand association and dissociation from the heme, as well as the kinetics of oxidation−reduction reactions occurring at the heme site. We present herein a detailed biochemical and spectroscopic characterization of purified human recombinant Cgb.

MATERIALS AND METHODS

Preparation of Recombinant Human Cgb and Its Mutants. The open reading frame of cloned human Cgb cDNA was synthesized by PCR using oligonucleotide primers, designed to incorporate the *Nde*I and *Bgl*II restriction sites at the 5′ and 3′ ends of the gene, respectively. They were cloned into the Novagen expression vector pET15b (six-His tag) at the *Nde*I and *Bam*HI sites to generate constructs for recombinant protein. Cgb fused with the six-His tag was expressed in *E. coli* BL21(DE3) cells (Stratagene) that were cultured overnight in LB medium supplemented with 1 mM isopropyl 1-thio-β-D-galactopyranoside (Wako Pure Chemical Co., Osaka, Japan) and 0.5 mM δ-aminolevulinic acid (Sigma). Cgb was purified with nickel−NTA agarose resin (Qiagen, Valencia, CA). The six-His tag was cleaved by using a thrombin cleavage capture kit (Novagen). The protein thus purified was subjected to 12.5% SDS−PAGE as shown in Figure 1B, to verify that recombinant human Cgb was in a highly pure form. The mutagenesis of Cgb, in which six histidine residues were replaced with alanine or glycine (H65A, H81A, H97A, H113A, H117A, H161A, H81G, and H81A/H113A), was carried out by PCR using mutated primers. The sequences of the mutated DNA were determined using the Pharmacia Express sequencer. Expression, purification, and identification of the Cgb mutants were the same as those for the wild-type protein. The concentration of Cgb was determined by the pyridine hemochromogen method (*18*). The ferrous−CO complexes of wild-type Cgb and the mutants were prepared by adding a small amount of solid dithionite to the Cgb solution in the CO atmosphere. The oxy complex was prepared by reduction of the ferric iron with ascorbic acid under aerobic conditions.

Electrochemical Experiments. A working gold mesh electrode (40 mm × 9 mm × 0.7 mm) was immersed in the optical cell. A platinum wire and Ag/AgCl (3 M KCl) electrodes were used as auxiliary and reference electrodes, respectively. The potential was controlled by a potentiostat (HA-301, HokutoDenko Co.). Optical absorption spectra were recorded on a U-3300 Hitachi UV−vis spectrophotometer during electronic reduction and oxidation. For the electrochemical redo titration, the following redox mediator dyes (5 mM each) were added to the sample solution [the $E_{1/2}$ values (vs NHE) of the mediator dyes are shown in parentheses] (*19*, *20*): 2,6-dichloroindophenol sodium salt (215 mV), indophenol (160 mV), phenazine methosulfate (80 mV), gallocyanine (20 mV), indigo trisulfonate (−80 mV), 2-hydroxy-1,4-naphthoquinone (−120 mV), anthraquinone-2-sulfonate (−230 mV), and benzyl viologen (−350 mV). The Cgb solution containing the mediator dyes was repeatedly degassed and flushed with argon prior to the measurement, and ∼2.5 mL of the sample solution was then transferred to the electrochemical cell, which was sealed with a rubber septum, by using a gastight syringe under an argon atmosphere. The electrochemical cell was kept in a thermoelectric cell holder of the spectrophotometer at 15 °C during the electrochemical titration. The absorbance change in the regions of the Soret and Q-bands was recorded as a measure of the redox reaction of Cgb.

Spectroscopies. Recombinant Cgb was dissolved in 50 mM Tris-HCl buffer containing 100 mM NaCl at pH 8.0 for spectroscopic measurements. The optical absorption spectra were obtained at room temperature using a UV-2500PC UV−vis spectrophotometer (Simadzu), and CD spectra were obtained with a JASCO J-725 CD instrument over the range of 190−250 nm (Figure 1C). The samples (5 μM) were placed in a 1 mm quartz cell at room temperature, and their spectra were scanned with a 1 nm band-pass with a time constant of 0.5 s.

Resonance Raman spectra were measured with a JASCO NR-1800 spectrometer (Japan) in the single-dispersion mode, which was equipped with a liquid nitrogen-cooled CCD detector (Princeton Instruments). The slit width for the spectral measurements was 4 cm^{-1}. The excitation wavelengths used for measurements of the ferric, ferrous (deoxy), ferrous−CO, and ferrous−O_2 complexes of the protein were 413 nm from a krypton ion laser (Coherent, Innova 90). The cylindrical Raman cell containing a ∼30 μM sample solution was spun to minimize local heating and photodissociation of the iron-bound CO or O_2. The spectrum of the CO photodissociation product of Cgb was measured using a nonspinning cell by excitation with 413 (Kr^+) and 441 nm light from a He−Cd vapor laser (KIMMOM, Elect. Co. Ltd.). The power of the Kr^+ laser and He−Cd laser at the sample was ∼10−50 mW. Holographic filters (Kaiser Optical Systems, Inc.) were used to eliminate the Rayleigh scattering. The Raman spectrometer was calibrated for each measurement using indene as the standard. Infrared spectra were measured using a SPECTRUM 2000 spectrometer (Perkin-Elmer Inc.). Approximately 20 μL of the solution was applied to the CaF_2 IR cuvette.

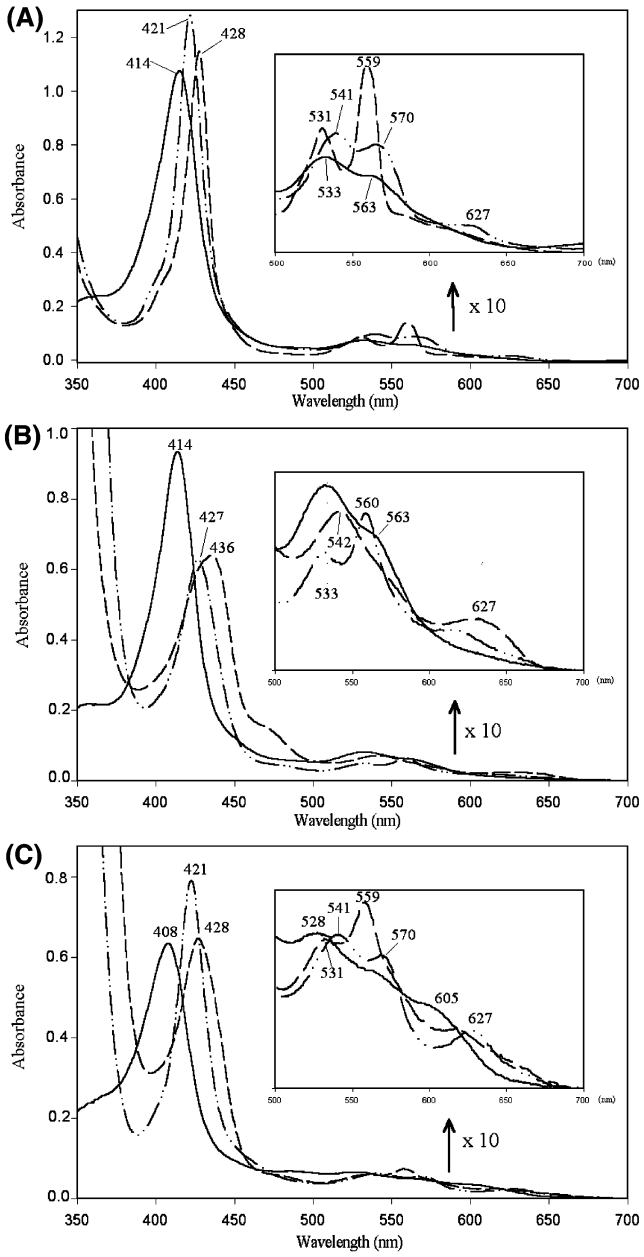

FIGURE 2: Absorption spectra of wild-type (WT) (A), H81A (B), and H113A (C) Cgb. Their spectra in the ferric, ferrous, and ferrous−CO complexes are represented by a solid line, a dashed line, and a dashed and dotted line, respectively. The proteins (~10 μM) were dissolved in 50 mM Tris-HCl buffer at pH 8.0.

RESULTS

CD and Absorption Spectra of Cgb and Its Mutants. We obtained a recombinant protein of human Cgb in highly purified form. Its CD spectrum (Figure 1C) had double minima at 209 and 222 nm, an indication of the α-helical protein of Cgb. On the basis of the spectral property, the α-helical content was estimated to be 72%. This high value is comparable to those of members of the globin family such as Mb (76%) or those of the highly helical protein such as the four-helix bundle (>80%) (*21*, *22*). In light of the sequence alignment (Figure 1A), Cgb possibly belongs to the globin family.

The optical absorption spectra of Cgb were measured in ferric, ferrous (deoxy), and ferrous−CO states (Figure 2A). These spectra resemble those of some hemoproteins having a hexacoordinated iron (*23*, *24*). In particular, the spectral features of deoxy Cgb, which displays large amplitudes of the α-band at 559 nm and the Soret band at 428 nm, are characteristic of a heme iron with two histidyl imidazoles as axial ligands (His−Fe−His). In the sequence alignment of Cgb with some globin proteins (Figure 1A), we anticipated that His113 and His81 would correspond to the F8 and E7 residues in globins, respectively.

To directly examine the coordination structure of the heme iron, six single mutants of Cgb were prepared by replacing the six histidine residues with alanine, the resultant mutants being designated as H65A, H81A, H97A, H113A, H117A, and H161A, and their optical absorption spectra were measured in the ferric, ferrous, and ferrous−CO states. As we expected, the H113A and H81A mutants exhibited spectral properties that were different from those of the wild-type (WT) protein (Figure 2B,C), while the spectra of the others were the same as that of the WT protein (data not shown). The spectrum of the H113A mutant in the ferric state suggests a His−Fe^{3+}−H_2O/OH^- structure, and the spectrum of H81A in the deoxy state was characteristic of the pentacoordinated His−Fe^{2+} form. These results apparently suggest that His81 and His113 are involved in coordination to the heme iron of Cgb as axial ligands.

However, it is interesting to note that the spectra of the deoxy H113A and ferric H81A mutants are indicative of hexacoordinate and low-spin iron, apparently similar (but not identical) to those of the corresponding states of WT Cgb. One possible explanation for these observations is ligand switching associated with a change in the iron oxidation state, e.g., His113−Fe^{3+}−X ↔ His81−Fe^{2+}−X, similar to the heme-based CO sensor protein CooA, in which the coordination structure changes between the Pro2−Fe^{3+}−Cys75 form and the Pro2−Fe^{2+}−His77 form (*25*). Another explanation is that this might be a secondary effect of the His mutation of Cgb; that is, non-native ligands could occupy the vacant coordination position of the iron after the His81 or His113 mutation.

To address these issues, we examined spectral changes in Cgb during redox titration using electrochemical techniques. In the case of CooA, the potential value for the reduction step ($Fe^{3+} \rightarrow Fe^{2+}$) was −320 mV, while that of the oxidation step ($Fe^{2+} \rightarrow Fe^{3+}$) was −260 mV. The redox potentials of CooA differed by 60 mV between the oxidation and reduction steps, although the spectral changes are completely identical in both steps. This could be explained by the redox-dependent ligand switching; the thiolate anion (S^-) from Cys75, which stabilizes the ferric state, is replaced with the neutral imidazole of His77, which would contribute stabilization of the ferrous state.

This is not the case for Cgb. The spectral change was fully reversible between the ferric and ferrous (deoxy) forms of Cgb. The Nernst plots in Figure 3A are also completely overlapped in the forward (reduction) and reverse (oxidation) steps, which gave 20 mV (vs NHE) of the redox potential for Cgb. The potential value indicates that the axial ligands of the heme iron in Cgb would be electronically neutral. On the basis of these results on the redox titration, it is suggested that the ligands of Cgb need not be switched, depending on the iron oxidation states, and that a His81−Fe−His113 form is, therefore, the most possible

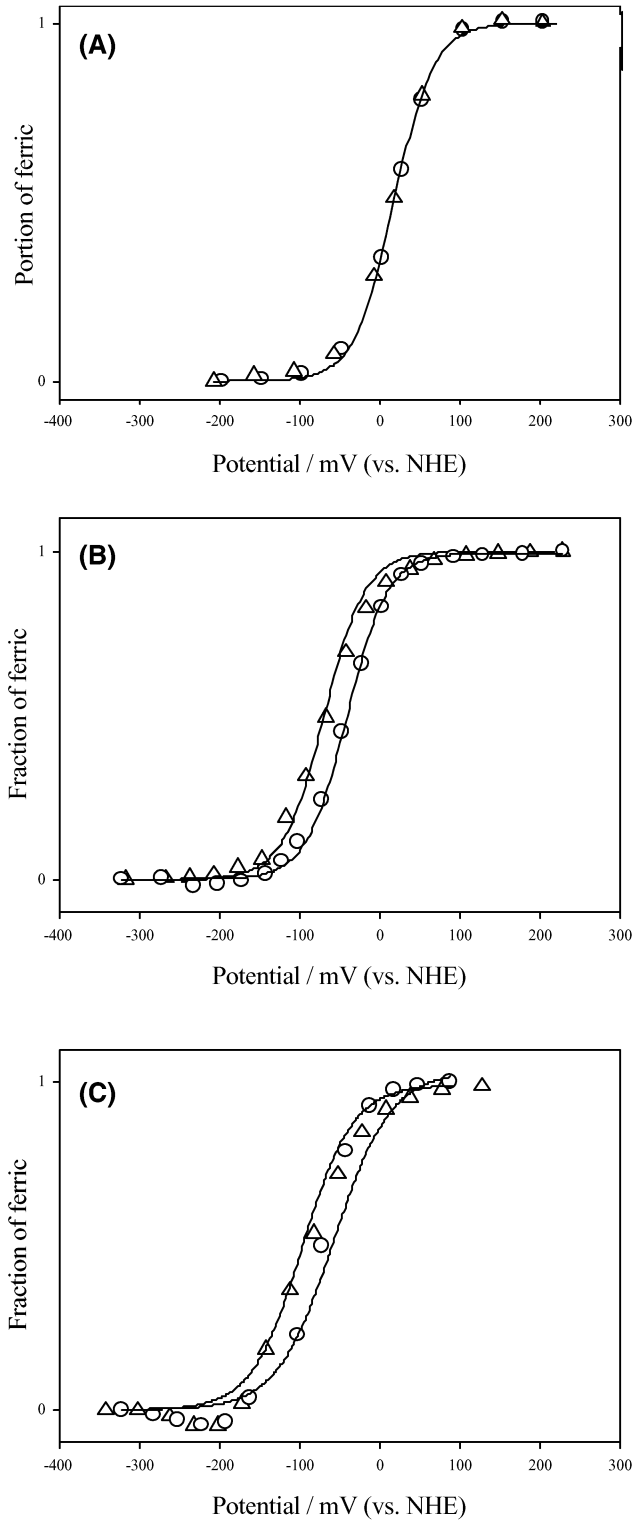

FIGURE 3: Nernst plots of reductive (△) and oxidative (○) titration of (A) WT, (B) H81A, and (C) H113A Cgb. The fraction of the ferric form was plotted as a function of the applied potential. Individual data points are an average of at least three independent measurements. The solid lines are theoretical Nernst curves for a one-electron reduction (△) and oxidation (○).

coordination structure in the ferric and ferrous (deoxy) states. This suggestion was supported by the resonance Raman and IR spectral results of the H81A and H113A mutants of Cgb, as described below. In addition, we observed that the heme could not be incorporated into the double mutant, H81A/H113A, of Cgb (data not shown).

On the other hand, the redox titration of H81A and H113A mutants exhibited a hysteresis in the reduction and oxidation steps, as shown in panels B and C of Figure 3. In addition, their midpoint potentials (−80 to −90 mV) are different from that of WT Cgb. As is the case for CooA, slow redox-dependent ligand switching was observed in these two mutants of Cgb, apparently consistent with optical absorption spectral observations (Figure 2A,B). Either Cys83 or Met86, each of which may be located close to His81 (see Figure 1A), is a candidate of the non-native sixth ligand in the mutants. It should also be noted that His117 is present after one helical turn from His113 in the F helix. Therefore, the distal and proximal pockets of Cgb might be flexible, and these residues might occupy the vacant coordination position after His81 or His113 is replaced with alanine, resulting in the hexacoordination structure for deoxy His113Ala and ferric His81Ala mutants, as described above. Similar observations already have been made in other cases, for example, in truncated Hb from *Chlamydomonas eugametos* (K87A and Y63L mutants) and *Synechocystis* Hb (H46A mutant) (*26*, *27*).

Resonance Raman and IR Spectra of Cgb. To characterize the coordination structure of Cgb in more detail, the resonance Raman spectra were obtained, since the high-frequency regions of hemoproteins are composed of porphyrin in-plane vibrational modes. The ν_4 and ν_3 lines serve as sensitive markers of the oxidation state and the coordination/spin state of the heme iron, respectively (*28*−*30*). Spectra a and b of Figure 4A show the Raman spectra of Cgb in the ferric and deoxy states, respectively. The marker lines ν_4 and ν_3 in the spectrum of the ferric form were located at 1375 and 1507 cm^{-1}, respectively, while those in the spectrum of the deoxy form are found at 1361 and 1493 cm^{-1}, respectively. These spectral features are characteristic of hemoproteins in the hexacoordinate and low-spin iron (*28*, *31*, *32*). The spectra of the ferric and deoxy proteins were invariant with a change in pH over the range of 5−8.

The ν_4 and ν_3 lines of the ferrous−CO ($Fe^{2+}CO$) complex of Cgb were located at 1374 and 1497 cm^{-1}, respectively, showing that the complex is also in the hexacoordinate and low-spin state (spectrum c of Figure 4A(c)). In the low-frequency region (Figure 4B), isotope-sensitive lines were detected and assigned as Fe−C−O modes. The lines in the region of 490−520 cm^{-1} were decomposed into three lines at 518 (50%), 510 (10%), and 492 cm^{-1} (40%). Upon substitution with $^{13}C^{18}O$, these three bands were shifted to 506, 497, and 480 cm^{-1}, respectively. These were assigned to the ν_{Fe-CO} stretching modes, since the frequencies and isotopic shifts of these lines were consistent with those observed for the ν_{Fe-CO} stretching modes of other hemoproteins. Another isotope-sensitive line observed at 584 cm^{-1} (562 cm^{-1} with $^{13}C^{18}O$) was assigned to the ν_{Fe-C-O} bending mode.

We also measured the IR spectra of Cgb in the ferrous−CO complex (Figure 5a). Three bands arising from ν_{C-O} stretching are observed at 1930 (∼50%), 1946 (∼10%), and 1971 cm^{-1} (∼40%), which were shifted to 1880, 1858, and 1843 cm^{-1}, respectively, upon substitution of $^{13}C^{18}O$ for $^{12}C^{16}O$. It is well-known that an inverse correlation exists between the frequencies of the ν_{Fe-CO} stretching modes and the ν_{C-O} stretching modes of ferrous−CO complexes of many hemoproteins and heme model compounds (*33*−*35*).

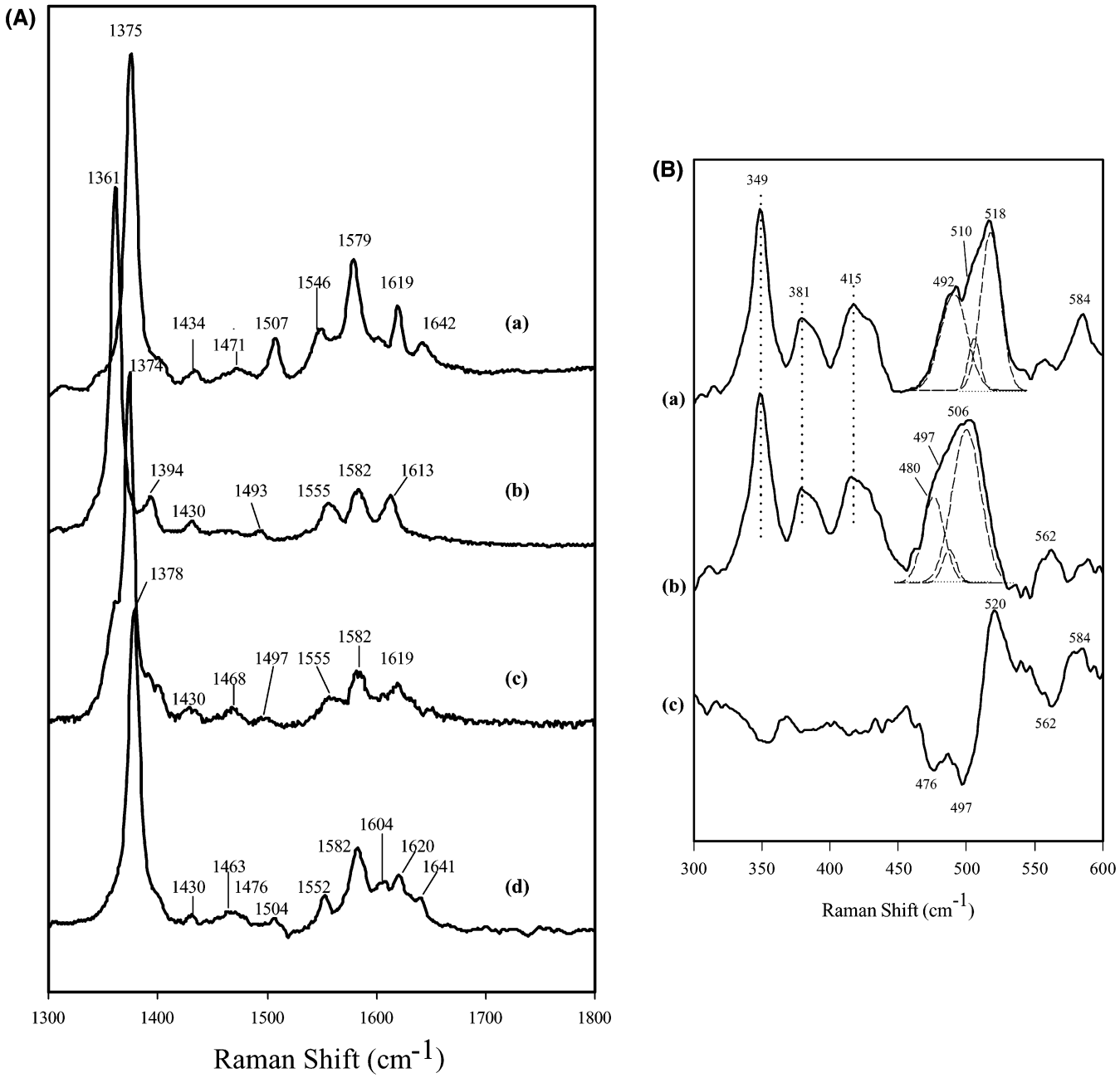

FIGURE 4: (A) Resonance Raman spectra of Cgb in the high-frequency region in the (a) ferric (Fe^{3+}), (b) ferrous (Fe^{2+}), (c) ferrous−CO (Fe^{2+}−CO), and (d) ferrous−O_2 (Fe^{2+}−O_2) forms. The spectra were obtained using a laser wavelength of 413 nm with a power of ∼50 mW. The buffer was 50 mM Tris-HCl at pH 8.0. (B) Resonance Raman spectra of the Fe^{2+}−CO form of Cgb in the low-frequency region: (a) $Fe^{12}C^{16}O$, (b) $Fe^{13}C^{18}O$, and (c) difference spectrum ($Fe^{12}C^{16}O$ − $Fe^{13}C^{18}O$). The dotted lines show the spectra obtained by the spectral deconvolution.

Since the origin of this relation is π-electron back-donation from the dπ (d_{xz}, d_{yz}) orbitals of the iron to the empty π^* orbitals of CO, the bond order between iron and CO increases as the bond order between the carbon and oxygen atoms of CO decreases and vice versa. Depending on the nature of the proximal ligand or the absence of a fifth ligand, different correlation lines are observed, due to differences in the charge on the iron atoms that reflect the strength of the Fe−CO bond (*36*). Since Cgb is a hemoprotein with a His−Fe−CO structure, its ν_{Fe-CO} versus ν_{C-O} plot would be expected to be on the line for many hemoproteins having a histidyl imidazole at the site opposite the CO coordination. On the basis of this ν_{Fe-CO} versus ν_{C-O} correlation (Figure 6), we suggest three configurations in the CO coordination to the iron of Cgb, the ν_{Fe-CO} and ν_{C-O} pairs which are at 518 and 1930 cm^{-1}, 492 and 1971 cm^{-1}, and 510 and 1946 cm^{-1}.

Spectra b and c of Figure 5 also show the IR spectra of the CO complexes of the H81A and H113A mutants of Cgb, respectively. In the H81A spectrum, only one ν_{C-O} stretching band was observed at 1971 cm^{-1} (1880 cm^{-1} for the $^{13}C^{18}O$ complex). A spectral comparison between the WT and the H81A mutant of Cgb clearly indicated that the two bands at 1930 and 1946 cm^{-1} had disappeared with a concomitant increase in the magnitude of the band at 1971 cm^{-1} (1880 cm^{-1} with $^{13}C^{18}O$) in the case of the His81 mutation. We obtained the same result in the H81G mutant of Cgb (data not shown). On the other hand, the ν_{C-O} band for the H113A mutant was located at 1963 cm^{-1} (1871 cm^{-1} with $^{13}C^{18}O$),

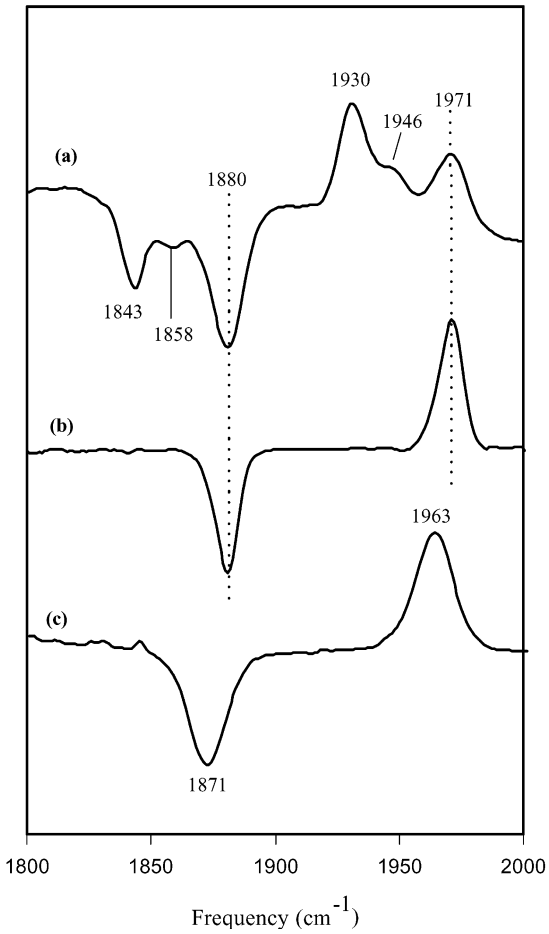

FIGURE 5: C−O stretching region of the FTIR spectra of the Fe^{2+}−CO form of (a) WT, (b) H81A, and (c) H113A Cgb. The spectra are representative of the form of the difference spectra between the $Fe^{12}C^{16}O$ and $Fe^{13}C^{18}O$ complexes. They were measured at room temperature in 50 mM Tris-HCl and 100 mM NaCl at pH 8.0.

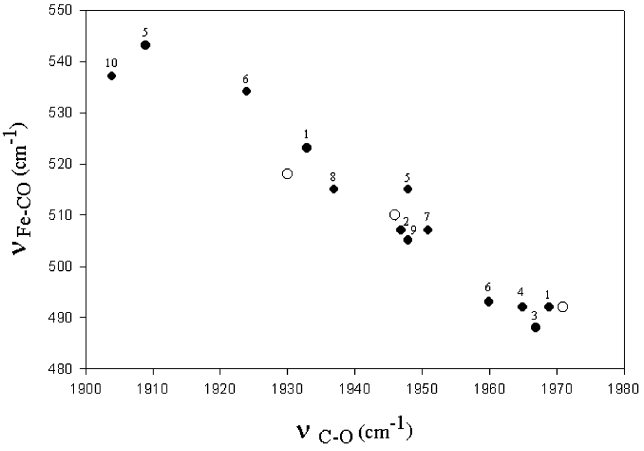

FIGURE 6: Correlation between the frequencies of the ν_{Fe-CO} stretching modes and the ν_{C-O} stretching modes for various heme proteins having a histidine residue as their proximal ligand. Empty circles represent data for Cgb, while filled circles represent data for (1) mouse Ngb, (2) sperm whale Mb (neutral pH), (3) sperm whale Mb (low pH), (4) the His64Gly mutant of sperm whale Mb, (5) *Ascaris suum* Hb, (6) barley Hb, (7) human HbA, (8) elephant Mb, (9) leghemoglobin, and (10) horseradish peroxidase.

the position of which is entirely different from that of the WT protein, indicating that the Fe−CO bond character and its surrounding environment in the H113A mutant are

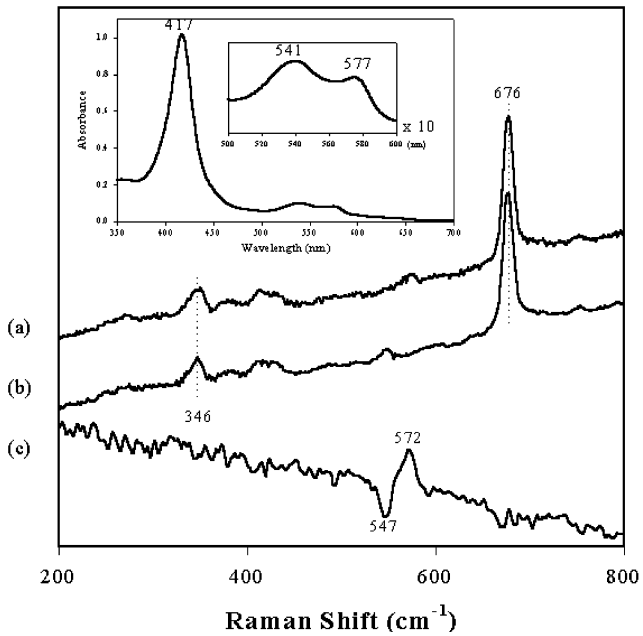

FIGURE 7: Resonance Raman spectra of the $Fe^{2+}-O_2$ complex of Cgb: (a) $^{16}O_2$, (b) $^{18}O_2$, and (c) $^{16}O_2$ minus $^{18}O_2$ difference spectra. The inset is the optical absorption spectrum of the oxy complex of Cgb. The oxy complex was prepared in 50 mM Tris-HCl and 100 mM NaCl at pH 8.0.

completely different from those in WT Cgb. The ν_{Fe-CO} lines for the H81A and H113A mutants were observed at 492 and 497 cm^{-1}, respectively, in their resonance Raman spectra (data not shown). The ν_{Fe-CO} versus ν_{C-O} correlation suggested that the positions opposite the bound CO are occupied by histidyl imidazoles for both Cgb mutants. In the H81A mutant, CO binds to the heme iron in the E helix (distal) side, as is the case for the WT protein, while CO possibly binds in the F helix (proximal) side of the H113A mutant.

In Cgb, CO binds to the heme iron at the sixth position after the His81 imidazole dissociates. In addition, it should also be noted that the dissociated His81 imidazole in the ferrous−CO complex of Cgb could occupy a position identical to that of the distal E7 histidine in Mb and Hb and that the ν_{C-O} stretching bands observed at 1930 and 1946 cm^{-1} possibly arise from the bound CO interacting with the dissociated His81 imidazole, while the CO responsible for the ν_{C-O} band at 1971 cm^{-1} is free from such interactions.

We also attempted to characterize the coordination structure of the O_2 complex of Cgb via optical and resonance Raman spectroscopic techniques. In the presence of ascorbic acid, the O_2 complex of Cgb that was prepared was sufficiently stable ($\tau_{1/2}$ much longer than several hours) against autoxidation to permit the spectrum to be obtained. Its optical absorption spectral feature bore good resemblance to the corresponding ones of oxy complexes of many globins (inset of Figure 7). In the Raman spectra, the ν_4 and ν_3 lines were located at 1378 and 1504 cm^{-1}, respectively, and the ν_{Fe-OO} stretching mode of Cgb was detected at 572 cm^{-1} (547 cm^{-1} for the $^{18}O_2$ complex), as illustrated in Figure 7. The frequency of the ν_{Fe-OO} stretching mode of Cgb was similar to those of elephant Mb (572 cm^{-1}), Ngb (571 cm^{-1}), and Mb (569 cm^{-1}) (*37*−*39*), rather than those of *Chlamydomonas* Hb (554 cm^{-1}), *Paramecium* Hb (563 cm^{-1}), *Mycobacterium tuberculosis* Hb (560 cm^{-1}), and *Syn-*

echocystis Hb (554 cm^{-1}) (*40*−*42*). The differences in the ν_{Fe-OO} stretching mode have been explained in terms of differences in the hydrogen bonding interaction site of the iron-bound O_2: the distal oxygen atom is hydrogen bonded in the case of the higher-frequency group (*43*). In the spectrum of the O_2 complex of Cgb, the ν_8 stretching mode, which has been reported to involve the bending motions of peripheral substituents of porphyrin, is located at 346 cm^{-1}. In the spectral comparison between the CO and O_2 complexes [the ν_8 band at 349 cm^{-1} for the CO complex (Figure 4B)], it was found that the ν_8 band was shifted by 3 cm^{-1} upon replacement of O_2 with CO. This observation is quite similar to that for Mb (2 cm^{-1} shift) but is comparable to that of HemAT-Bs (11 cm^{-1} shift) (*44*−*46*). Since the stretching mode is believed to be sensitive to structural changes that occur in the distal side of the heme pocket upon ligand binding, it is likely to suggest that the heme pocket structure in the distal side of Cgb is essentially similar between these two complexes, as is the case for Mb, but not for HemAT-Bs.

DISCUSSION

Bis-Histidine Binding to Ferric and Deoxy Cgb. We report here the first detailed characterization of the heme pocket structure of the fourth human globin, Cgb. The spectroscopic results for WT and mutants of Cgb presented here unambiguously show that His113 (F8) and His81 (E7) in Cgb bind to the iron as the fifth and sixth axial ligands, respectively. The heme iron in Cgb is bis-histidyl hexacoordinate in the low-spin state, essentially the same as that of Ngb, but not Mb and Hb. However, a striking difference in the heme environmental structure between Cgb and Ngb is evident from redox potential measurements. The potential value is 20 mV for Cgb in the ferric/ferrous couple, while it is −129 mV for Ngb (*17*). This difference in the redox property is directly related to the structural and functional differences between these two globins. In functional aspects, the difference in the redox potential is possibly responsible for the difference in stability of their oxy (O_2-bound) complexes; the oxy complex of Cgb is quite stable, while that of Ngb is readily autoxidized to the ferric state (*16*, *17*).

It is noteworthy that the redox potential value (20 mV) of Cgb is comparable to that of cytochrome b_5 (29 mV) (*47*), which also contains a *b*-type heme with bis-histidyl hexacoordination. In the crystal structure of cyt b_5, the imidazole NH groups of the histidine ligands (His39 and His61) are weakly hydrogen bonded to the main chain carbonyl oxygen atoms of Gly42 and Phe58, respectively, resulting in them having a neutral character. Therefore, it is likely, in the case of Cgb, that the heme axial imidazoles of His81 and His113 are electronically neutral, possibly due to weak hydrogen bonding of their imidazole NH groups with their surroundings. In sharp contrast, histidyl imidazole ligand(s) in Ngb must be anionic, as a result of strong hydrogen bonding interactions with their surroundings. To directly compare the Fe−His bond characters (ν_{Fe-His}) between Cgb and Ngb, we attempted to measure the resonance Raman spectrum of the CO-photodissociated product of Cgb. Couture et al. recently reported on the ν_{Fe-His} stretching frequency of Ngb after photodissociation of CO from the ferrous−CO complex, which is weak in its intensity but located at 225 cm^{-1} (*38*). However, in the spectra of Cgb measured using 442 or 413 nm excitation, the hexacoordinated species was dominant rather than the CO photodissociated pentacoordinate product, and as a result, the ν_{Fe-His} band was not detected, most probably due to less effective CO photodissociation or its rapid rebinding.

Recently, the association (k_{-H}) and dissociation (k_H) rate constants of the internal imidazole ligand in CO flash photolysis experiments have been reported and compared between histoglobin (=Cgb) (*3*) and Ngb (*16*): $k_{-H} \sim 5\ s^{-1}$ and $k_H = 430\ s^{-1}$ for the former protein, while $k_{-H} = 8200\ s^{-1}$ (2000 s^{-1}) and $k_H = 9800\ s^{-1}$ (4.5 s^{-1}) for the later protein (values in parentheses were reported in ref *17*). Such a difference in the kinetic properties may reflect differences in the electronic structure of the histidyl imidazole ligands and/or electronic environment of the heme pocket between Cgb and Ngb. This is highly related to kinetic parameters in binding of the external CO ligand between the two globins, which will be discussed in the next section.

External Ligand Binding to Cgb. Mb and Hb are in the pentacoordinate and high-spin state in their ferrous (deoxy) form, which leaves the sixth position empty and available for the binding of exogenous ligands such as CO and O_2. On the other hand, in the hexacoordinate and low-spin forms of ferrous (deoxy) globins found in invertebrates and nonsymbiotic plants, the presence of a sixth ligand to the iron interferes with exogenous ligand binding (*24*, *25*). Cgb is not an exception to this. As evidenced by the IR study (see Figure 5), the CO ligand ejects the His81 imidazole from the sixth coordination position and occupies this position. On the basis of the IR (ν_{C-O}) and resonance Raman (ν_{Fe-CO}) spectral data, we propose that there are three conformers (conformational isomers) concerning the CO coordination to Cgb: the ν_{Fe-CO} and ν_{C-O} pairs are 518 and 1930 cm^{-1}, 510 and 1946 cm^{-1}, and 492 and 1971 cm^{-1}. These conformers arise from differences in the degree of interaction of the iron-bound CO with its surroundings. In particular, electrostatic interactions with charged groups have been considered to be major factors that affect Fe−C−O bond characteristics. When a positively charged group is present close to the iron-bound CO, an $Fe{=}C{=}O\cdots X^+$ structure is stabilized, in which the Fe−CO and C−O bonds have double bond character. On the other hand, a negatively charged group stabilizes an $Fe{-}C{\equiv}O^{\delta+}\cdots X^-$ structure, in which the Fe−CO bond tends toward single bond character and the C−O bond tends toward triple bond character (*48*).

The ν_{Fe-CO} and ν_{C-O} modes of the conformers in Cgb are basically the same as those reported in Ngb, except for the second (510 and 1946 cm^{-1}) conformer, because two conformers (523 and 1933 cm^{-1} and 492 and 1969 cm^{-1}) have been observed in the CO complex of Ngb (*38*). The first (518 and 1930 cm^{-1}) and the second (510 and 1946 cm^{-1}) conformers of Cgb can be assigned to closed conformations, where a positively charged group(s) near the iron-bound CO stabilizes the $Fe{=}C{=}O\cdots X^+$ structure. On the basis of the IR spectral results for the WT and H81A mutant (see Figure 5), X^+ would be predicted to be the imidazole of His81 that occupies the distal (E7) position of Mb. The second conformer exhibits ν_{Fe-CO} and ν_{C-O} modes identical to those (507 and 1947 cm^{-1}) of Mb, although the concentration of this fraction is minor (∼10%). In this conformer, the $Fe{=}C{=}O\cdots$His81 configuration should be

similar to that of Mb. On the other hand, the ν_{Fe-CO} and ν_{C-O} stretching modes for the first conformer suggest that electrostatic and/or hydrogen bonding interactions in the Fe═C═O···X^+ form are more numerous in Cgb than in Mb. Not only His81 (E7) but also another positively charged residue would be involved in the interaction. As is the case for Lys67 in Ngb, Arg84 of Cgb may occupy the E11 position and may contribute to this interaction. On the other hand, Rovira et al. suggested, on the basis of the theoretical calculation, that two different conformations of His E7 imidazole give two different interactions with the iron-bound CO, which could exhibit the ν_{C-O} stretching mode at 1930 and 1946 cm^{-1} (*49*). Although it is known that O_2 is less sensitive than CO to electrostatic interactions, the frequency of the ν_{Fe-OO} stretching mode of the oxy complex indicates that the heme-bound O_2 in Cgb is stabilized through a hydrogen bond between the distal oxygen atom and its surroundings, possibly with the His81 imidazole and/or Arg84.

The third form (492 and 1971 cm^{-1}) of the CO complex of Cgb, whose population is ≤40%, can be unambiguously assigned as an open structure where no group is sufficiently close to the iron-bound CO to affect the electronic structure of the Fe−C−O unit, like Mb at low pH (488 and 1967 cm^{-1}), where the distal histidine becomes protonated and swings out of the pocket. The H64G mutant of Mb (492 and 1965 cm^{-1}) is also a good model of the open heme pocket in the third conformers of Cgb. Indeed, the H81A and H81G (data not shown) mutants of Cgb gave ν_{Fe-CO} and ν_{C-O} stretching modes at 492 and 1971 cm^{-1}, respectively, suggesting the open heme pocket structure for the third conformer of the CO complex of Cgb.

The heme environmental structure of Cgb must be highly related to the equilibrium and kinetic properties of the external ligand bindings. Most recently, kinetic studies of O_2 and CO binding to human histoglobin (=Cgb) were reported by Trent et al. (*3*): $k_{on} = 30\ \mu M^{-1}\ s^{-1}$, $k_{off} = 0.35\ s^{-1}$, and $K = 1.0\ \mu M^{-1}$ for O_2 binding and $k_{on} = 5.6\ \mu M^{-1}\ s^{-1}$, $k_{off} = 0.003\ s^{-1}$, and $K = 21.7\ \mu M^{-1}$ for CO binding. Compared to the equilibrium and kinetic rates of Mb ($k_{on} = 17\ \mu M^{-1}\ s^{-1}$, $k_{off} = 15\ s^{-1}$, and $K = 1.1\ \mu M^{-1}$ for O_2 binding and $k_{on} = 0.51\ \mu M^{-1}\ s^{-1}$, $k_{off} = 0.02\ s^{-1}$, and $K = 25.5\ \mu M^{-1}$ for CO binding), the ligand association is more rapid and the dissociation is slower. This comparison is consistent with the heme pocket structure characterized in this study on the basis of the vibrational spectral data: 40% open conformer mainly contributes the fast ligand binding, and the bound ligands are stabilized through specific interaction with the distal residues. Despite such differences in the kinetic parameters, the equilibrium constants for O_2 and CO binding are the same for Cgb and Mb, since coordination of the sixth His81 ligand could control the affinity of the heme iron of Cgb toward O_2 and CO. Consequently, Cgb exhibits the same affinities of the heme iron for the ligands as Mb. In contrast, since structures in the Fe−C−O unit are essentially similar, as stated above, the kinetic properties of Ngb ($k_{on} = 130\ \mu M^{-1}\ s^{-1}$ and $k_{off} = 0.3\ s^{-1}$ for O_2 binding and $k_{on} = 38\ \mu M^{-1}\ s^{-1}$ and $k_{off} = 0.007\ s^{-1}$ for CO binding) are apparently similar to those of Cgb. However, the equilibrium constants of Ngb ($K = 200\ \mu M^{-1}$ for O_2 binding and $K = 2500\ \mu M^{-1}$ for CO binding) are much different than those of Cgb. This is mainly caused by large differences in the kinetic parameters (k_{-H} and k_H) for internal His81 binding. As stated before, differences in the electronic structure of the histidyl imidazole(s) between the two mammalian hexacoordinate globins are responsible for differences in their equilibrium and kinetic properties, as well as in their redox potential and autoxidation rate. In functional aspects, Cgb is much more useful as an O_2 reservoir than Ngb, because the O_2 affinity is on the same order of magnitude as that of Mb, and the resultant oxy form is sufficiently stable to autoxidation. Cgb is dramatically induced in fibrotic liver. Since the circulation of the blood does not run smoothly in the fibrotic tissues, Cgb may play a part as an O_2 reservoir in tissues lacking O_2.

ACKNOWLEDGMENT

We thank Dr. Eiji Obayashi for his support in measurements of resonance Raman and IR spectra.

REFERENCES

1. Kawada, N., Kristensen, D. B., Asahina, K., Nakatani, K., Minamiyama, Y., Seki, S., and Yoshizato, K. (2001) *J. Biol. Chem. 276*, 25318−25323.
2. Kristensen, D. B., Kawada, N., Asahina, K., Nakatani, K., Minamiyama, Y., Seki, S., and Yoshizato, K. (2000) *Hepatology 32*, 268−277.
3. Trent, J. T., III, and Hargrove, M. S. (2002) *J. Biol. Chem. 277*, 19538−19545.
4. Burmester, T., Ebner, B., Weich, B., and Hankeln, T. (2002) *Mol. Biol. Evol. 19*, 416−421.
5. Awenius, C., Hankeln, T., and Burmester, T. (2001) *Biochem. Biophys. Res. Commun. 287*, 418−421.
6. Burmester, T., Welch, B., Reinhardt, S., and Hankeln, T. (2000) *Nature 407*, 520−523.
7. Couture, M., Das, T., Savard, P., Oullet, Y., and Wittenberg, J. (1999) *J. Biol. Chem. 274*, 6898−6910.
8. Scoot, N., and LeComte, J. (2000) *Protein Sci. 3*, 587−597.
9. Couture, M., Das, T., Savard, P., Ouellet, Y., Wittenberg, B., Jr., Rousseau, D., and Guertin, M. (2000) *Eur. J. Biochem. 267*, 4770−4780.
10. Hvitved, A. N., Trent, J. T., III, Premer, S. A., and Hargrove, M. S. (2001) *J. Biol. Chem. 274*, 748−754.
11. Arredondo-Peter, R., Hargrove, M. S., Moran, J. F., Sarath, G., and Klucas, R. V. (1998) *Plant Physiol. 118*, 1121−1125.
12. Hunt, P. W., Watts, R. A., Trevaskis, B., Llewellyn, D. J., Burnell, J., Dennis, E. S., and Peacock, W. J. (2001) *Plant Mol. Biol. 47*, 677−692.
13. Hargrove, M. S., Brucker, E. A., Boguslaw, S., Gantam, S., and Phillip, G. N., Jr. (2000) *Structure 8*, 1005−1014.
14. Taylor, E. R., Nie, X. Z., Alexander, W. M., and Hill, R. D. (1994) *Plant Mol. Biol. 24*, 853−862.
15. Trevaskis, B., Watts, R. A., Anderson, C. R., Llewellyn, D. J., Hargrove, M. S., Olson, J. S., Dennis, E. S., and Peacock, W. J. (1997) *Proc. Natl. Acad. Sci. U.S.A. 94*, 12230−12234.
16. Trent, J. T., III, Watts, R. A., and Hargrove, M. S. (2001) *J. Biol. Chem. 276*, 30106−30110.
17. Dewilde, S., Kiger, L., Burmester, T., Hankeln, T., Baudin-Creuza, V., Aerts, T., Marden, M. C., Caubergs, R., and Moens, L. (2001) *J. Biol. Chem. 276*, 38949−38955.
18. Paul, K.-G., Theorell, H., and Akeson, A. (1953) *Acta Chem. Scand. 7*, 1284−1289.
19. Zahn, J. A., Arciero, D. M., Hooper, A. B., and Dispirito, A. A. (1996) *Eur. J. Biochem. 240*, 684−691.
20. Baymann, F., Moss, D. A., and Mäntele, W. (1991) *Anal. Biochem. 199*, 269−274.
21. Isogai, Y., Ota, M., Fujisawa, T., Izuno, H., Mukai, M., Nakamura, H., Iizuka, T., and Nisikawa, K. (1999) *Biochemistry 38*, 7431−7443.
22. Gibrey, B. R., Rabanal, F., Reddy, K. S., and Dutton, P. L. (1998) *Biochemistry 37*, 4635−4643.
23. Arredondo-Peter, R., Hargrove, M. S., Sarath, G., Moran, J. F., Lohrman, J., Olson, J. S., and Klncas, R. V. (1997) *Plant Physiol. 115*, 1259−1266.

24. Duff, S. M. G., Wittenberg, J. B., and Hill, R. D. (1997) *J. Biol. Chem. 272*, 16746−16752.
25. Nakajima, H., Honma, Y., Tawara, T., Kato, T., Park, S.-Y., Miyatake, H., Shiro, Y., and Aono, S. (2001) *J. Biol. Chem. 276*, 7055−7061.
26. Das, T. K., Couture, M., Lee, H. C., Peisach, J., Rousseau, D. L., Wittenberg, B. A., Wittenberg, J. B., and Guertin, M. (1999) *Biochemistry 38*, 15360−15368.
27. Couture, M., Das, T. K., Savard, P.-Y., Ouellet, Y., Wittenberg, J. B., Wittenberg, B. A., Rousseau, D. L., and Guertin, M. (2000) *Eur. J. Biochem. 267*, 4770−4780.
28. Spiro, T. G., and Li, X. Y. (1988) in *Biological Applications of Raman Spectroscopy* (Spiro, T. G., Ed.) Vol. 3, pp 1−37, John Wiley & Sons, New York.
29. Hu, S., Smith, K. S., and Spiro, T. G. (1996) *J. Am. Chem. Soc. 118*, 12638−12646.
30. Wang, J., Caughey, W. S., and Rousseau, D. L. (1996) in *Methods in Nitric Oxide Research* (Feelisch, M., and Stamler, J., Eds.) pp 427−454, John Wiley & Sons, New York.
31. Das, T. K., Lee, H. C., Duff, S. M., Hill, R. D., Peisach, J., Rousseau, D. L., Wittenberg, B. A., and Wittenberg, J. B. (1999) *J. Biol. Chem. 274*, 4207−4212.
32. Vogel, K. M., Spiro, T. G., Shelver, D., Thorsteinsson, M. V., and Roberts, G. P. (1999) *Biochemistry 38*, 2679−2687.
33. Park, K. D., Guo, K. M., Adebodun, F., Chiu, M. L., Sligar, S. G., and Oldfield, E. (1991) *Biochemistry 30*, 2333−2347.
34. Ray, G. B., Li, X. Y., Ibers, J. A., Sessler, J. L., and Spiro, T. G. (1994) *J. Am. Chem. Soc. 116*, 162−176.
35. Das, T. K., Friedman, J. M., Kloek, A. P., Goldberg, D. E., and Rousseau, D. L. (2000) *Biochemistry 39*, 837−842.
36. Wang, J., Stuehr, D. J., and Rousseau, D. L. (1997) *Biochemistry 36*, 4595−4606.
37. Kerr, E. A., Yu, N.-T., Bartnicki, D. E., and Mizukami, H. (1985) *J. Biol. Chem. 260*, 8360−8365.
38. Couture, M., Burmester, T., Hankeln, T., and Rousseau, D. L. (2001) *J. Biol. Chem. 276*, 36377−36382.
39. Van Wart, H. E., and Zimmer, J. (1985) *J. Biol. Chem. 260*, 8372−8377.
40. Das, T. K., Couture, M., Ouellet, Y., Guertin, M., and Rousseau, D. L. (2001) *Proc. Natl. Acad. Sci. U.S.A. 98*, 479−484.
41. Das, T. K., Weber, R. E., Dewilde, S., Wittenberg, J. B., Wittenberg, B. A., Yamauchi, K., Van Hauwaert, M. L., Moens, L., and Rousseau, D. L. (2000) *Biochemistry 39*, 14330−14340.
42. Yeh, S. R., Couture, M., Ouellet, Y., Guertin, M., and Rosseau, D. L. (2000) *J. Biol. Chem. 275*, 1679−1684.
43. Rousseau, D. L., and Friedman, J. M. (1988) in *Biological Application of Raman Spectroscopy* (Spiro, T. G., Ed.) Vol. 3, pp 133−215, John Wiley & Sons, New York.
44. Hirota, S., Ogura, T., Appelman, E. H., Shinzawa-Itoh, K., Yoshikawa, S., and Kitagawa, T. (1994) *J. Am. Chem. Soc. 116*, 10564−10570.
45. Hirota, S., Ogura, T., Shinzawa-Ito, K., Yoshikawa, S., Nagai, M., and Kitagawa, T. (1994) *J. Phys. Chem. 98*, 6652−6660.
46. Aono, S., Kato, T., Matsuki, M., Nakajima, H., Ohta, T., Uchida, T., and Kitagawa, T. (2002) *J. Biol. Chem. 277*, 13528−13538.
47. Velick, S. F., and Strittmatter, P. (1956) *J. Biol. Chem. 221*, 265−275.
48. Phillip, G. N., Jr., Teodoro, M. L., Li, T., Smith, B., and Olson, J. S. (1999) *J. Phys. Chem. B 103*, 8817−8829.
49. Rovia, C., Schulze, B., Eichiger, M., Evanseck, J. D., and Parrinello, M. (2001) *Biophys. J. 81*, 435−445.

BI027067E